

---

# Multifidelity Reinforcement Learning with Control Variates

---

Anonymous Author(s)

Affiliation

Address

email

## Abstract

1        In many computational science and engineering applications, the output of a  
2        system of interest corresponding to a given input can be queried at different  
3        levels of fidelity with different costs. Typically, low-fidelity data is cheap and  
4        abundant, while high-fidelity data is expensive and scarce. In this work we study  
5        the reinforcement learning (RL) problem in the presence of multiple environments  
6        with different levels of fidelity for a given control task. We focus on improving  
7        the RL agent’s performance with multifidelity data. Specifically, a multifidelity  
8        estimator that exploits the cross-correlations between the low- and high-fidelity  
9        returns is proposed to reduce the variance in the estimation of the state-action  
10       value function. The proposed estimator, which is based on the method of control  
11       variates, is used to design a multifidelity Monte Carlo RL (MFMCR) algorithm that  
12       improves the learning of the agent in the high-fidelity environment. The impacts of  
13       variance reduction on policy evaluation and policy improvement are theoretically  
14       analyzed by using probability bounds. Our theoretical analysis and numerical  
15       experiments demonstrate that for a finite budget of high-fidelity data samples,  
16       our proposed MFMCR agent attains superior performance compared with that of a  
17       standard RL agent that uses only the high-fidelity environment data for learning  
18       the optimal policy.

## 19    1 Introduction

20    Within the computational science and engineering (CSE) community, multifidelity data refers to  
21    data that comes from different sources with different levels of fidelity. The criteria by which data is  
22    considered to be low fidelity or high fidelity vary across different applications, but usually low-fidelity  
23    data is much cheaper to generate than high-fidelity data under some cost metric. In robotics for  
24    instance, data coming from a robot operating in the real world constitutes high-fidelity data, while  
25    simulated data of the robot based on first principles is considered to be low-fidelity data. Different  
26    simulators of the robot can also be designed by increasing the modeling complexity. A simulator  
27    that takes into account aerodynamic drag is, for instance, of higher fidelity than one that is based  
28    only on the simple laws of motion. As another example, a neural classifier in deep learning can be  
29    trained on the *full* training data for a *large* number of training epochs, or on a *subset* of the training  
30    data for *few* epochs. Evaluating the trained model on a held-out validation data set in the former  
31    case yields a higher-fidelity estimate of the classifiers’ performance compared with that in the latter  
32    case. In general, low-fidelity data serves as an approximation to its high-fidelity counterpart and  
33    can be generated cheaply and abundantly [24]. Many outer-loop applications that require querying  
34    the system at many different inputs, including black-box optimization [21], inference [29], and  
35    uncertainty propagation [19, 27], can exploit the cross-correlations between low- and high-fidelity  
36    data to solve new problems that would otherwise be prohibitively costly to solve using high-fidelity  
37    data alone [28, 29].

38 Motivated by the advent of multifidelity data sources within CSE, in this work we study the rein-  
 39 forcement learning (RL) problem in the presence of multiple environments with different levels of  
 40 fidelity for a given control task. RL is a popular machine learning paradigm for intelligent sequential  
 41 decision-making under uncertainty, enabling data-driven control of complex systems with scales  
 42 ranging from quantum [18] to cosmological [26]. State-of-the-art model-free RL algorithms have  
 43 indeed demonstrated sheer success for learning complex policies from raw data in single-fidelity  
 44 environments [25, 22, 31, 32, 12]. This success, however, comes at the cost of requiring a large num-  
 45 ber of data samples to solve a control task *satisfactorily*.<sup>1</sup> In the presence of multiple environments  
 46 with different levels of fidelity, new ways arise that could help the agent learn better policies. One  
 47 way that has been well studied in the context of RL is *transfer learning (TL)*. In TL [35, 8, 39], the  
 48 agent first uses the low-fidelity environment to learn a policy that is then transferred (directly or  
 49 indirectly through the transfer of the state-action value function) to the high-fidelity environment  
 50 as a heuristic to bootstrap learning. Essentially, TL attempts to leverage multifidelity environments  
 51 to deal with the exploration-exploitation dilemma that is present within RL, and it works under the  
 52 assumption that the maximum deviation between the optimal low-fidelity state-action value function  
 53 and the optimal high-fidelity state-action value function is bounded with a threshold that is used  
 54 by TL for bootstrapping the high-fidelity value function [9]. In our work we explore an uncharted  
 55 territory and focus on *multifidelity* estimation in RL and its role in improving the learning of the  
 56 agent. We demonstrate that as long as the low- and high-fidelity state-action value functions for  
 57 any policy are correlated, significant performance improvements can be reaped by leveraging these  
 58 cross-correlations without extra effort in managing the exploration-exploitation process.

59 The main contributions of our work are summarized as follows. First, we study a generic multifidelity  
 60 setup in which the RL agent can execute a policy in two environments, a low-fidelity environment  
 61 and a high-fidelity environment. To leverage the cross-correlations between the low- and high-fidelity  
 62 returns, we propose an unbiased reduced-variance multifidelity estimator for the state-action value  
 63 function based on the framework of control variates. Second, a multifidelity Monte Carlo (MC) RL  
 64 algorithm, named MFMCRL, is proposed to improve the learning of the RL agent in the high-fidelity  
 65 environment. For any finite budget of high-fidelity environment interactions, MFMCRL leverages  
 66 low-fidelity data to learn better policies than a standard RL agent that uses only the high-fidelity  
 67 data. Third, we theoretically analyze the impacts of variance reduction in the estimation of the state-  
 68 action value function on policy evaluation and policy improvement using probability bounds. Fourth,  
 69 performance gains of the proposed MFMCRL algorithm are empirically assessed through numerical  
 70 experiments in synthetic multifidelity environments, as well as a neural architecture search (NAS)  
 71 use case.

## 72 2 Preliminaries and related work

### 73 2.1 Reinforcement learning

74 We consider episodic RL problems where the environment  $\Sigma$  is specified by an infinite-horizon  
 75 Markov decision process (MDP) with discounted returns [5]. Specifically, an infinite-horizon MDP  
 76 is defined as a tuple  $\mathcal{M} = (\mathcal{S}, \mathcal{A}, \mathcal{P}, \beta, \mathcal{R}, \gamma)$ , where  $\mathcal{S}$  and  $\mathcal{A}$  are finite sets of states and actions,  
 77 respectively;  $\mathcal{P} : \mathcal{S} \times \mathcal{A} \times \mathcal{S} \rightarrow [0, 1]$  is the environment dynamics; and  $\beta : \mathcal{S} \rightarrow [0, 1]$  is the  
 78 initial distribution over the states, that is,  $\beta(s) = \Pr(s_0 = s), \forall s \in \mathcal{S}$ . The reward function  $\mathcal{R}$  is  
 79 bounded and defined as  $\mathcal{R} : \mathcal{S} \times \mathcal{A} \rightarrow [R_{\min}, R_{\max}]$ , where  $R_{\min}$  and  $R_{\max}$  are real numbers.  $\gamma$  is a  
 80 discount factor to bound the cumulative rewards and trade off how far- or short-sighted the agent is  
 81 in its decision making. The environment dynamics,  $\mathcal{P}(s'|s, a), \forall s, a, s' \in \mathcal{S} \times \mathcal{A} \times \mathcal{S}$ , encode the  
 82 stationary transition probability from a state  $s$  to a state  $s'$  given that action  $a$  is chosen [7, 16]. In the  
 83 episodic setting, there exists at least one terminal state  $s_T$  such that  $\mathcal{P}(s'|s_T, a) = 0, \forall a, s' \neq s_T$  and  
 84  $\mathcal{P}(s_T|s_T, a) = 1, \forall a$ , i.e.  $s_T$  is an absorbing state. Furthermore,  $\beta(s_T) = 0$  and  $\mathcal{R}(s_T, a) = 0, \forall a$ .  
 85 When the RL agent transitions into a terminal state, all subsequent rewards are zero, and simulation  
 86 is restarted from another state  $s \sim \beta$ .

87 The agent’s decision-making process is characterized by  $\pi(a|s)$ , which is a Markov stationary policy  
 88 that defines a distribution over the actions  $a \in \mathcal{A}$  given a state  $s \in \mathcal{S}$ . In the RL problem,  $\mathcal{P}$

<sup>1</sup>Poor sample complexity of model-free RL algorithms has long motivated developments in model-based RL, where a predictive model of the environment is learned alongside the policy [14, 30]. Our work is focused on model-free RL.

89 and  $\mathcal{R}$  are not known to the agent, yet the agent can interact with the environment sequentially  
90 at discrete time steps,  $t = 0, 1, 2, \dots, T$ , by exchanging actions and rewards. Notice that  $T$  is a  
91 random variable and denotes the time step at which the agent transitions into a terminal state. At  
92 each time step  $t$ , the agent observes the environment's state  $s_t = s \in \mathcal{S}$ , takes action  $a_t = a \sim$   
93  $\pi(a|s) \in \mathcal{A}$ , and receives a reward  $r_{t+1} = \mathcal{R}(s, a)$ . The environment's state then evolves to a  
94 new state  $s_{t+1} = s' \sim \mathcal{P}(s'|s, a)$ . The state-value function of a state  $s$  under a policy  $\pi$  is defined  
95 as the expected long-term discounted returns starting in state  $s$  and following policy  $\pi$  thereafter,  
96  $V_\pi(s) = \mathbb{E}_{a_t \sim \pi, s_t \sim \mathcal{P}} \left[ \sum_{t=0}^{\infty} \gamma^t \mathcal{R}(s_t, a_t) | s_0 = s \right]$ . In addition, the state-action value function of a  
97 state  $s$  and action  $a$  under a policy  $\pi$  is defined as  $Q_\pi(s, a) = \mathbb{E}_{a_t \sim \pi, s_t \sim \mathcal{P}} \left[ \sum_{t=0}^{\infty} \gamma^t \mathcal{R}(s_t, a_t) | s_0 = \right.$   
98  $s, a_0 = a \left. \right]$ . Notice that  $V_\pi(s) = \mathbb{E}_{a \sim \pi} [Q_\pi(s, a)]$ . The solution of the RL problem is a policy  $\pi^*$  that  
99 maximizes the discounted returns from the initial state distribution  $\pi^* = \operatorname{argmax}_{\pi} \mathbb{E}_{s \sim \beta} [V_\pi(s)]$ . It is  
100 well known that there exists at least one optimal policy  $\pi^*$  such that  $V_{\pi^*}(s) = \max_{\pi} V_\pi(s), \forall s \in \mathcal{S}$   
101 and  $Q_{\pi^*}(s, a) = \max_{\pi} Q_\pi(s, a), \forall s, a \in \mathcal{S} \times \mathcal{A}$  [2]. Furthermore, a deterministic policy that selects  
102 the greedy action with respect to  $Q_{\pi^*}(s, a), \forall s \in \mathcal{S}$ , is an optimal policy.

## 103 2.2 Control variates

104 The method of control variates is a variance reduction technique that leverages the correlation  
105 between random variables (r.v.s.) to reduce the variance of an estimator [20]. Let  $W_1, W_2, \dots, W_n$   
106 be  $n$  independent and identically distributed (i.i.d.) r.v.s. such that  $\mathbb{E}[W_i] = \mu_w$ , and  $\mathbb{E}[(W_i -$   
107  $\mu_w)^2] = \sigma_w^2, \forall i \in [n]$ . In addition, let  $Z_1, Z_2, \dots, Z_n$  be  $n$  i.i.d. r.v.s. such that  $\mathbb{E}[Z_i] = \mu_z$ , and  
108  $\mathbb{E}[(Z_i - \mu_z)^2] = \sigma_z^2, \forall i \in [n]$ . Suppose that  $W_i, Z_i$  are correlated with a correlation coefficient  
109  $\rho_{w,z} = \frac{\operatorname{Cov}[Z_i, W_i]}{\sqrt{\sigma_z^2} \sqrt{\sigma_w^2}}, \forall i \in [n]$ , where  $\operatorname{Cov}[Z_i, W_i] = \mathbb{E}[Z_i W_i] - \mathbb{E}[Z_i] \mathbb{E}[W_i]$  is the covariance  
110 between  $Z_i$  and  $W_i$ . Furthermore, suppose that  $W_i, Z_j$  are independent and thus uncorrelated  $\forall i \neq j$ .  
111 Using the Cauchy—Schwartz inequality, one can show that  $|\rho_{w,z}| \leq 1$ .

112 To estimate  $\mu_w$ , we first consider the sample mean estimator,  $\hat{\theta}_1 = \frac{1}{n} \sum_{i=1}^n W_i$ .  $\hat{\theta}_1$  is an unbiased  
113 estimator of  $\mu_w$ , in other words,  $\mathbb{E}[\hat{\theta}_1] = \frac{1}{n} \sum_{i=1}^n \mathbb{E}[W_i] = \mu_w$ , and has a variance  $\operatorname{Var}[\hat{\theta}_1] = \frac{\sigma_w^2}{n}$ .  
114 Next, we consider the control-variate-based estimator,

$$\hat{\theta}_2 = \frac{1}{n} \sum_{i=1}^n W_i + \alpha(Z_i - \mu_z). \quad (1)$$

115  $\hat{\theta}_2$  is also an unbiased estimator of  $\mu_w$ , i.e.,  $\mathbb{E}[\hat{\theta}_2] = \mu_w$ , yet it has a variance  $\operatorname{Var}[\hat{\theta}_2] = \frac{1}{n} \operatorname{Var}[W_i +$   
116  $\alpha(Z_i - \mu_z)] = \frac{1}{n} (\operatorname{Var}[W_i] + \alpha^2 \operatorname{Var}[Z_i] + 2\alpha \operatorname{Cov}[Z_i, W_i])$ . The variance of  $\hat{\theta}_2$  can be controlled and  
117 minimized by setting  $\alpha$  to the minima of  $\operatorname{Var}[W_i] + \alpha^2 \operatorname{Var}[Z_i] + 2\alpha \operatorname{Cov}[Z_i, W_i]$ , which is attained  
118 at  $\alpha^* = -\frac{\operatorname{Cov}[Z_i, W_i]}{\sigma_z^2} = -\rho_{z,w} \frac{\sigma_w}{\sigma_z}$ . Hence, by introducing  $\alpha(Z_i - \mu_z)$  as a control variate, the  
119 variance of  $\hat{\theta}_2$  is reduced,

$$\operatorname{Var}[\hat{\theta}_2] = (1 - \rho_{z,w}^2) \operatorname{Var}[\hat{\theta}_1]. \quad (2)$$

120 Because  $\hat{\theta}_2$  is an unbiased estimator,  $\hat{\theta}_2$  has a lower mean squared error (MSE) by the bias-variance  
121 decomposition theorem of the MSE. Applications of the method of control variates extend beyond  
122 variance reduction. For example, the concept of control variates is used in [27] to design a fusion  
123 framework to combine an arbitrary number of surrogate models optimally.

## 124 2.3 Related work

125 In [1], a policy search algorithm is proposed that leverages a crude approximate model  $\hat{\mathcal{P}}$  of the true  
126 MDP to quickly learn to perform well on real systems. The proposed algorithm, however, is limited  
127 to the case where  $\mathcal{P}$  is deterministic, and it assumes that model derivatives are good approximations  
128 of the true derivatives such that policy gradients can be computed by using the approximate model.

129 In transfer learning (TL) [36, 23], value, model, or policy parameters are transferred in one direction  
130 as a heuristic initialization to bootstrap learning in the high-fidelity environment, with no option  
131 for backtracking. The option for the agent to backtrack and to choose which environment to use is  
132 studied in the multifidelity RL (MFRL) work of [9]. That algorithm is extended in [33] by integrating  
133 function approximation using Gaussian processes [38]. As in TL, both [9] and [33] use the value  
134 function from a lower-fidelity environment as a heuristic to bootstrap learning and *guide exploration*  
135 in the high-fidelity environment. From an optimization viewpoint, this approach is reasonable only  
136 if the lower-fidelity value function lies in the vicinity of the optimal high-fidelity value function, a  
137 situation that cannot be guaranteed or known a priori in general. Hence, in [9, 33], it is assumed that  
138 the optimal state-action value function in the low- and high-fidelity environments differ by no more  
139 than a small parameter  $\beta$  at every state-action pair, and they require the knowledge of  $\beta$  a priori to  
140 manage exploration-exploitation across multifidelity environments. By contrast, we require only that  
141 the low- and high-fidelity returns are correlated in our work, and the correlation need not be known  
142 a priori. The cross-correlation between the low- and high-fidelity returns is used for reducing the  
143 variance in the *estimation* of the high-fidelity state-action value function, and hence our approach is  
144 complementary to existing TL techniques that use multifidelity environments for guided exploration  
145 [9, 33]. We show that as long as the low- and high-fidelity state-action value function of a policy are  
146 correlated, the agent can benefit from the cheap and abundantly available low-fidelity data to improve  
147 its performance, without altering the exploration process.

### 148 3 Multifidelity estimation in RL

#### 149 3.1 Problem setup

150 We consider a multifidelity setup in which the RL agent has access to two environments,  $\Sigma^{\text{lo}}$  and  $\Sigma^{\text{hi}}$ ,  
151 modeled by the two MDPs  $\mathcal{M}^{\text{lo}} = (\mathcal{S}^{\text{lo}}, \mathcal{A}, \mathcal{P}^{\text{lo}}, \beta^{\text{lo}}, \mathcal{R}^{\text{lo}}, \gamma)$ , and  $\mathcal{M}^{\text{hi}} = (\mathcal{S}^{\text{hi}}, \mathcal{A}, \mathcal{P}^{\text{hi}}, \beta^{\text{hi}}, \mathcal{R}^{\text{hi}}, \gamma)$ ,  
152 respectively, as shown in Figure 1.  $\Sigma^{\text{lo}}$  is a low-fidelity environment in which the low-fidelity  
153 reward function  $\mathcal{R}^{\text{lo}} : \mathcal{S} \times \mathcal{A} \rightarrow [R_{\min}^{\text{lo}}, R_{\max}^{\text{lo}}]$  and the low-fidelity dynamics  $\mathcal{P}^{\text{lo}}$  are cheap<sup>2</sup> to  
154 evaluate/simulate, yet they are potentially inaccurate. On the other hand,  $\Sigma^{\text{hi}}$  is a high-fidelity  
155 environment in which the high-fidelity reward function  $\mathcal{R}^{\text{hi}} : \mathcal{S} \times \mathcal{A} \rightarrow [R_{\min}^{\text{hi}}, R_{\max}^{\text{hi}}]$  and the high-  
156 fidelity dynamics  $\mathcal{P}^{\text{hi}}$  describe the real-world system with the highest accuracy, yet they are expensive  
157 to evaluate/simulate [11]. We stress that  $(\mathcal{P}^{\text{hi}}, \beta^{\text{hi}}, \mathcal{R}^{\text{hi}})$  and  $(\mathcal{P}^{\text{lo}}, \beta^{\text{lo}}, \mathcal{R}^{\text{lo}})$  are **unknown** to the agent,  
158 and interaction with the two environments is only through the exchange of states, actions, next states  
159 and rewards, which is the typical case in RL.

160 The action space  $\mathcal{A}$  is the same in both environments, yet the state space may differ. It is assumed  
161 that the low-fidelity state space is a subset of the high-fidelity state space,  $\mathcal{S}^{\text{lo}} \subseteq \mathcal{S}^{\text{hi}}$ , in other words,  
162 the states available in the low-fidelity environment are a subset of those available at the high-fidelity  
163 environment, and it is assumed that there exists a known mapping<sup>3</sup>  $\mathcal{T} : \mathcal{S}^{\text{hi}} \rightarrow \mathcal{S}^{\text{lo}}$  as in previous  
164 works [36, 9]. High-fidelity environments usually capture more state information than do low- fidelity  
165 environments so  $\mathcal{T}$  can be a many-to-one map. Access to the high-fidelity simulator  $\Sigma^{\text{hi}}$  is restricted  
166 to full episodes  $\tau^{\text{hi}} = (s_0^{\text{hi}}, a_0, r_1^{\text{hi}}, s_1^{\text{hi}}, a_1, r_2^{\text{hi}}, s_2^{\text{hi}}, \dots, s_T^{\text{hi}})$ . On the other hand,  $\Sigma^{\text{lo}}$  is generative, and  
167 simulation can be started by the agent at any state-action pair [15, 17]. Using  $\mathcal{T}$  and  $\Sigma^{\text{lo}}$ , the agent  
168 can map a  $\tau^{\text{hi}}$  to  $\tau^{\text{lo}} = (\mathcal{T}(s_0^{\text{hi}}), a_0, r_1^{\text{lo}}, \mathcal{T}(s_1^{\text{hi}}), a_1, r_2^{\text{lo}}, \mathcal{T}(s_2^{\text{hi}}), \dots, \mathcal{T}(s_T^{\text{hi}}))$ , and it is assumed that  
169  $\Pr(\tau^{\text{lo}}) > 0$  under  $\mathcal{P}^{\text{lo}}$  and  $\beta^{\text{lo}}$ . It is also assumed that  $\mathcal{R}^{\text{lo}}(\mathcal{T}(s^{\text{hi}}), a)$  and  $\mathcal{R}^{\text{hi}}(s^{\text{hi}}, a)$  are correlated.

170 Based on this setup, a correlation exists between the low- and high- fidelity trajectories  
171 that can be beneficial for policy learning. In this work we study how to leverage the  
172 cheaply accessible low-fidelity trajectories from  $\Sigma^{\text{lo}}$ , to learn an optimal  $\pi^*$  that maximizes  
173  $\mathbb{E}_{s \sim \beta^{\text{hi}}} \left[ \mathbb{E}_{a_t \sim \pi, s_t \sim \mathcal{P}^{\text{hi}}} \left[ \sum_{t=0}^{\infty} \gamma^t \mathcal{R}^{\text{hi}}(s_t^{\text{hi}}, a_t) \mid s_0^{\text{hi}} = s \right] \right]$ ; in other words, to learn  $\pi^*$  that is optimal  
174 with respect to the high-fidelity environment  $\Sigma^{\text{hi}}$ .

<sup>2</sup>Sampling cost is application dependent. It is up to the practitioner to assign cost and determine low- and high-fidelity sampling budgets.

<sup>3</sup> $\mathcal{T}$  is problem-specific. For instance, if  $\mathcal{S}^{\text{hi}}$  represents a fine grid and  $\mathcal{S}^{\text{lo}}$  represents a coarse grid, then  $\mathcal{T}$  will map  $s^{\text{hi}}$  to the closest  $s^{\text{lo}}$  based on a chosen distance metric.

### 175 3.2 Multifidelity Monte Carlo RL

176 The Monte Carlo method to solve the RL problem is based on the idea of averaging sample  
 177 returns. In the MC method, experience is divided into episodes. At the end of an episode,  
 178 state-action values are estimated, and the policy is updated. For ease of exposition, we consider a  
 179 specific state-action pair  $(s^{\text{hi}}, a)$  in what follows and suppress the dependence on  $(s^{\text{hi}}, a)$  from  
 180 the notation to avoid clutter. Consider a sample trajectory  $\tau^{\text{hi}}$  that results from the agent's  
 181 interaction with the high-fidelity environment starting at  $(s_0^{\text{hi}} = s^{\text{hi}}, a_0 = a)$  and following  
 182  $\pi$ , that is,  $\tau^{\text{hi}} : s_0^{\text{hi}}, a_0, r_1^{\text{hi}}, s_1^{\text{hi}}, a_1, r_2^{\text{hi}}, \dots, s_T^{\text{hi}}$ .  
 183 Note that  $r_{t+1}^{\text{hi}} = \mathcal{R}^{\text{hi}}(s_t^{\text{hi}}, a_t)$ . Let  $\mathcal{G}^{\text{hi}}$  denote the corresponding long-term discounted return,  
 184  $\mathcal{G}^{\text{hi}} = \sum_{t=0}^{\infty} \gamma^t r_{t+1}^{\text{hi}}$ . The high-fidelity state-action value of the pair  $(s, a)$  when the agent follows  $\pi$   
 185 is

$$185 Q_{\pi}^{\text{hi}}(s^{\text{hi}}, a) = \mathbb{E}_{\tau^{\text{hi}}}[\mathcal{G}^{\text{hi}} | s_0^{\text{hi}} = s^{\text{hi}}, a_0 = a]. \quad (3)$$

186 Notice that  $Q_{\pi}^{\text{hi}}(s^{\text{hi}}, a)$  is the expectation of an r.v.  $\mathcal{G}^{\text{hi}}$  with respect to the random trajectory  $\tau^{\text{hi}}$ .  $\mathcal{G}^{\text{hi}}$   
 187 is a bounded r.v. with support on the interval  $[\frac{R_{\min}^{\text{hi}}}{1-\gamma}, \frac{R_{\max}^{\text{hi}}}{1-\gamma}]$  and has a finite variance given by

$$187 \sigma_{\text{hi}}^2(s^{\text{hi}}, a) = \mathbb{E}_{\tau^{\text{hi}}}[(\mathcal{G}^{\text{hi}} - Q_{\pi}^{\text{hi}}(s^{\text{hi}}, a))^2 | s_0 = s^{\text{hi}}, a_0 = a]. \quad (4)$$

188 By interacting with the environment, the agent can sample only a finite number of trajectories,  $n$ .  
 189 Let  $\tau_1^{\text{hi}}, \tau_2^{\text{hi}}, \dots, \tau_n^{\text{hi}}$  be the  $n$  sampled trajectories that starts at the pair  $(s^{\text{hi}}, a)$ . Furthermore, let  
 190  $\mathcal{G}_1^{\text{hi}}, \mathcal{G}_2^{\text{hi}}, \dots, \mathcal{G}_n^{\text{hi}}$  be i.i.d. r.v.s. that correspond to the long-term discounted returns of the sampled  
 191 trajectories,  $\tau_1^{\text{hi}}, \tau_2^{\text{hi}}, \dots, \tau_n^{\text{hi}}$ , respectively. Notice that  $\mathbb{E}_{\tau^{\text{hi}}}[\mathcal{G}_1^{\text{hi}}] = \mathbb{E}_{\tau^{\text{hi}}}[\mathcal{G}_2^{\text{hi}}] = \dots = \mathbb{E}_{\tau^{\text{hi}}}[\mathcal{G}_n^{\text{hi}}] =$   
 192  $Q_{\pi}^{\text{hi}}(s, a)$ . The first-visit MC sample average is

$$192 \hat{Q}_{\pi, n}^{\text{hi}}(s^{\text{hi}}, a) = \frac{1}{n} \sum_{i=1}^n \mathcal{G}_i^{\text{hi}}. \quad (5)$$

193 By the weak law of large numbers,  $\lim_{n \rightarrow \infty} \Pr(|\hat{Q}_{\pi, n}^{\text{hi}}(s^{\text{hi}}, a) - Q_{\pi}^{\text{hi}}(s^{\text{hi}}, a)| > \xi) = 0$ , for any positive  
 194 number  $\xi$ . In addition, the variance of this unbiased sample average estimator is

$$194 \text{Var}[\hat{Q}_{\pi, n}^{\text{hi}}(s^{\text{hi}}, a)] = \frac{\sigma_{\text{hi}}^2(s^{\text{hi}}, a)}{n}. \quad (6)$$

201 Using the low-fidelity generative environment and the method of control variates, we design an  
 202 unbiased estimator for the expected long-term discounted returns that has a smaller variance than  
 203 (6). Let  $\tau_i^{\text{lo}}$  be the  $i$ th low-fidelity trajectory that is obtained from  $\tau_i^{\text{hi}}$  by using  $\mathcal{T}$  and the generative  
 204 low-fidelity environment to evaluate  $r_{t+1}^{\text{lo}} = \mathcal{R}^{\text{lo}}(\mathcal{T}(s_t^{\text{hi}}), a_t)$ . Let  $\mathcal{G}_i^{\text{lo}}$  be the r.v. which corresponds to  
 205 the long-term discounted return of  $\tau_i^{\text{lo}}$ . Notice that  $\mathcal{G}_i^{\text{hi}}$  and  $\mathcal{G}_i^{\text{lo}}$  are correlated r.v.s. in this multifidelity  
 206 setup. Based on those low-fidelity trajectories, the low-fidelity first-visit MC sample average is  
 207  $\hat{Q}_{\pi, n}^{\text{lo}}(\mathcal{T}(s^{\text{hi}}), a) = \frac{1}{n} \sum_{i=1}^n \mathcal{G}_i^{\text{lo}}$  and has a variance of  $\text{Var}[\hat{Q}_{\pi, n}^{\text{lo}}(\mathcal{T}(s^{\text{hi}}), a)] = \frac{\sigma_{\text{lo}}^2(\mathcal{T}(s^{\text{hi}}), a)}{n}$ , where  
 208  $\sigma_{\text{lo}}^2(\mathcal{T}(s^{\text{hi}}), a) = \mathbb{E}_{\tau^{\text{lo}}}[(\mathcal{G}^{\text{lo}} - Q_{\pi}^{\text{lo}}(\mathcal{T}(s^{\text{hi}}), a))^2 | s_0 = \mathcal{T}(s^{\text{hi}}), a_0 = a]$  and  $Q_{\pi}^{\text{lo}}(\mathcal{T}(s^{\text{hi}}), a)$  is the true  
 209 population mean.

210 Using the method of control variates presented in Subsection 2.2, we propose the following multi-  
 211 fidelity MC estimator:

$$211 \hat{Q}_{\pi, n}^{\text{MFMC}}(s^{\text{hi}}, a) = \hat{Q}_{\pi, n}^{\text{hi}}(s^{\text{hi}}, a) + \alpha_{s, a}^* \left( Q_{\pi}^{\text{lo}}(\mathcal{T}(s^{\text{hi}}), a) - \hat{Q}_{\pi, n}^{\text{lo}}(\mathcal{T}(s^{\text{hi}}), a) \right), \quad (7)$$

212 where

$$\alpha_{s, a}^* = \frac{\text{Cov}[\hat{Q}_{\pi, n}^{\text{hi}}(s^{\text{hi}}, a), \hat{Q}_{\pi, n}^{\text{lo}}(\mathcal{T}(s^{\text{hi}}), a)]}{\text{Var}[\hat{Q}_{\pi, n}^{\text{lo}}(\mathcal{T}(s^{\text{hi}}), a)]}. \quad (8)$$

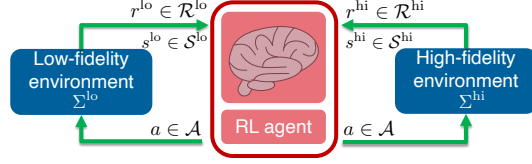


Figure 1: RL with low- and high-fidelity environments.  $\Sigma^{\text{lo}}$  is cheap to evaluate but is potentially inaccurate.  $\Sigma^{\text{hi}}$  represents the real world with the highest accuracy, yet it is expensive to evaluate. The RL agent leverages the correlations between the low- and high-fidelity data to learn  $\pi_{\text{hi}}^*$ .

213 Notice that the estimator in (7) is unbiased and has a variance of

$$\text{Var}\left[\hat{Q}_{\pi,n}^{\text{MFMC}}(s^{\text{hi}}, a)\right] = (1 - \rho_{s,a}^2) \text{Var}\left[\hat{Q}_{\pi,n}^{\text{hi}}(s^{\text{hi}}, a)\right], \quad (9)$$

214 where  $\rho_{s,a}$  is the correlation coefficient between the low-fidelity and high-fidelity long-term dis-  
215 counted returns:

$$\rho_{s,a} = \frac{\text{Cov}\left[\hat{Q}_{\pi,n}^{\text{hi}}(s^{\text{hi}}, a), \hat{Q}_{\pi,n}^{\text{lo}}(\mathcal{T}(s^{\text{hi}}), a)\right]}{\sqrt{\text{Var}\left[\hat{Q}_{\pi,n}^{\text{hi}}(s^{\text{hi}}, a)\right] \text{Var}\left[\hat{Q}_{\pi,n}^{\text{lo}}(\mathcal{T}(s^{\text{hi}}), a)\right]}}. \quad (10)$$

216 Therefore, the variance in estimating the value of a state-action pair under a policy  $\pi$  can be reduced  
217 by a factor of  $(1 - \rho_{s,a}^2)$  when the low-fidelity data is exploited, although the budget of high-fidelity  
218 samples remains the same. Notice that

$$\text{Cov}\left[\hat{Q}_{\pi,n}^{\text{hi}}(s^{\text{hi}}, a), \hat{Q}_{\pi,n}^{\text{lo}}(\mathcal{T}(s^{\text{hi}}), a)\right] = \text{Cov}\left[\frac{1}{n} \sum_{i=1}^n \mathcal{G}_i^{\text{hi}}, \frac{1}{n} \sum_{i=1}^n \mathcal{G}_i^{\text{lo}}\right] = \frac{1}{n} \text{Cov}\left[\mathcal{G}_i^{\text{hi}}, \mathcal{G}_i^{\text{lo}}\right], \quad (11)$$

219 because  $\mathcal{G}_i^{\text{hi}}, \mathcal{G}_j^{\text{lo}}$  are independent r.v.s.  $\forall i \neq j$ . Hence,  $\text{Cov}\left[\hat{Q}_{\pi,n}^{\text{hi}}(s^{\text{hi}}, a), \hat{Q}_{\pi,n}^{\text{lo}}(\mathcal{T}(s^{\text{hi}}), a)\right]$ ,  
220  $\text{Var}\left[\hat{Q}_{\pi,n}^{\text{hi}}(s^{\text{hi}}, a)\right]$ , and  $\text{Var}\left[\hat{Q}_{\pi,n}^{\text{lo}}(\mathcal{T}(s^{\text{hi}}), a)\right]$  can all be estimated in practice based on the return  
221 data samples using the standard unbiased estimators for the variance and covariance.

222 The reduced-variance estimator of (7) can be used to design a multifidelity Monte Carlo RL algorithm  
223 as shown in Algorithm 1 in Appendix A. This algorithm is based on the on-policy first-visit MC  
224 control algorithm with  $\epsilon$ -soft policies [34] but uses the multifidelity estimator (7). Algorithm 1 is  
225 based on the idea of generalized policy iteration. In the policy evaluation step (lines 11–18), the  
226 state-action value function is made consistent with the current policy by updating the estimated  
227 long-term discounted returns of a state-action pair  $(s_t, a_t)$  using the control-variate-based estimator  
228 (7) (line 18). This update requires the estimation of the correlation between the low- and high-  
229 fidelity returns, which is done in lines 13–17. Next, in the policy improvement step (lines 19–20), the  
230 policy is made  $\epsilon$ -greedy with respect to the current state-action value function. In each episode, the  
231 agent needs to evaluate the policy in the low-fidelity environment to obtain  $Q_{\pi}^{\text{lo}}$ . This can be done in  
232 practice by collecting a large number of  $m$  return samples from the cheap low-fidelity environment  
233 and setting  $Q_{\pi}^{\text{lo}}(\mathcal{T}(s^{\text{hi}}), a) \approx \hat{Q}_{\pi,m+n}^{\text{lo}}(\mathcal{T}(s^{\text{hi}}), a)$ . The convergence of Algorithm 1 to the optimal  
234  $\epsilon$ -greedy policy,  $\pi_{\epsilon-\text{opt}}^*$ , along with its corresponding  $\hat{Q}_{*}^{\text{MFMC}}$ , is guaranteed under the same conditions  
235 that guarantee convergence for the on-policy first-visit MC control algorithm with  $\epsilon$ -soft policies [34].  
236 In the following subsection, we theoretically analyze the impacts of variance reduction on policy  
237 evaluation and policy improvement.

### 238 3.3 Theoretical analysis

239 In this subsection we analyze the impacts of variance reduction on policy evaluation error and policy  
240 improvement by introducing two main theorems. Intermediate lemmas along with all the proofs can  
241 be found in Appendix B.

#### 242 3.3.1 Policy evaluation

243 In policy evaluation, the task is to estimate the state-action value function of a given policy  $\pi$ .  
244 Trajectory samples are first generated by interacting with the environment using  $\pi$ , and the state-action  
245 value function is then estimated using either the single high-fidelity estimator (5) or the proposed  
246 multifidelity estimator (7). To analyze the impacts of variance reduction on policy evaluation error,  
247 we first derive a Bernstein-type concentration inequality [6] that relates the deviation between the  
248 sample average and the true mean to the sample size  $n$ , estimation accuracy parameters  $\delta, \xi$ , and the  
249 variance of a r.v. as follows.

250 **Lemma 1** Let  $X_1, X_2, \dots, X_n$  be i.i.d. r.v.s. with mean  $\mathbb{E}[X_i] = \mu_x$  and variance  $\mathbb{E}[(X_i - \mu_x)^2] =$   
251  $\sigma_x^2, \forall i \in [n]$ . Furthermore, suppose that  $X_i, \forall i$ , are bounded almost surely with a parameter  $b$ ,  
252 namely,  $\Pr(|X_i - \mu_x| \leq b) = 1, \forall i$ . Then

$$\Pr\left(\left|\frac{1}{n} \sum_{i=1}^n X_i - \mu_x\right| \geq \xi\right) \leq 2 \exp\left(\frac{-n\xi^2}{4\sigma_x^2}\right) \quad (12)$$

253 for  $0 \leq \xi \leq \sigma_x^2/b$ .

254 Next, the concentration bound of Lemma 1 is used to derive the minimum sample size that is required  
 255 to ensure that the sample average deviates by no more than  $\xi$  from the true mean with high probability  
 256 for both the high-fidelity estimator (5) and the multifidelity estimator (7).

257 **Theorem 1** *To guarantee that*

258 1.  $Pr\left(|\hat{Q}_{\pi,n}^{hi}(s^{hi}, a) - Q_{\pi}^{hi}(s^{hi}, a)| \leq \xi\right) \geq 1 - \delta$ , then  $n \geq \frac{4\sigma_{hi}^2(s^{hi}, a)}{\xi^2} \log\left(\frac{2}{\delta}\right)$ .

259 2.  $Pr\left(|\hat{Q}_{\pi,n}^{MFMC}(s, a) - Q_{\pi}^{hi}(s^{hi}, a)| \leq \xi\right) \geq 1 - \delta$ , then  $n \geq \frac{4(1-\rho_{s,a}^2)\sigma_{hi}^2(s^{hi}, a)}{\xi^2} \log\left(\frac{2}{\delta}\right)$ .

260 The result of Theorem 1 highlights the benefit of using our proposed multifidelity estimator (7) for  
 261 policy evaluation as opposed to using the single high-fidelity estimator of (5). By leveraging the  
 262 correlation between low- and high-fidelity returns  $\rho_{s,a}$ , the variance of the multifidelity estimator  
 263 is reduced by a factor of  $(1 - \rho_{s,a}^2)$ , which makes it possible to achieve a low estimation error at a  
 264 reduced number of high-fidelity samples.

### 265 3.3.2 Policy improvement

266 In policy improvement, a new policy  $\pi'$  is constructed by deterministically choosing the greedy  
 267 action with respect to the state-action value function of the original policy  $\pi$ ,  $Q_{\pi}^{hi}(s, a)$ , at every state,  
 268 that is,  $\pi'(s) \doteq \operatorname{argmax}_{a \in \mathcal{A}} Q_{\pi}^{hi}(s, a)$ ,  $\forall s \in \mathcal{S}$ . By the policy improvement theorem,  $\pi'$  is as good as or

269 better than  $\pi$  under the assumption that  $Q_{\pi}^{hi}(s, a)$ ,  $\forall s, a$  is computed exactly. In practice, the MDP is  
 270 unknown, and the state-action value function is estimated based on a finite number of trajectories.  
 271 Moreover, those trajectories are generated by following an exploratory policy, such as an  $\epsilon$ -soft  
 272 policy. Because we are interested in studying how different estimators impact policy improvement,  
 273 we consider a target state  $s^{hi} \in \mathcal{S}^{hi}$  and assume that we have  $n$  trajectories for each action  $a \in \mathcal{A}$  at  
 274 this target state. This assumption basically ensures that all actions at the target state  $s^{hi}$  have been  
 275 explored equally well and enables us to make fair comparisons about estimator performance.

276 Without loss of generality, suppose that  $Q_{\pi}^{hi}(s^{hi}, a_1) \geq Q_{\pi}^{hi}(s^{hi}, a_2) \geq \dots \geq Q_{\pi}^{hi}(s^{hi}, a_{|\mathcal{A}|})$ . Let  $\Delta_i =$   
 277  $Q_{\pi}^{hi}(s^{hi}, a_1) - Q_{\pi}^{hi}(s^{hi}, a_i)$ ,  $\forall i \neq 1$ . We analyze the probability that  $a_1$ , which is the greedy action  
 278 given the true  $Q_{\pi}^{hi}(s^{hi}, a)$ , is the greedy action with respect to the single- and multifidelity estimators  
 279 in our next theorem.

280 **Theorem 2** *Suppose that the number of trajectories from a state-action pair at a target state  $s^{hi} \in \mathcal{S}^{hi}$*   
 281 *is the same for all actions  $a \in \mathcal{A}$  and that  $a_1$  is the greedy action with respect to the true  $Q_{\pi}^{hi}(s^{hi}, a)$ .*  
 282 *Furthermore, suppose that  $\mathcal{P}^{hi}(s^{hi} | s^{hi'}, a) \geq \beta(s^{hi})$ ,  $\forall s^{hi} \in \mathcal{S}^{hi}$ . Then*

283 1.  $Pr(a_1 = \operatorname{argmax}_{a \in \mathcal{A}} \hat{Q}_{\pi,n}^{hi}(s^{hi}, a)) \geq \prod_{i=2}^{|\mathcal{A}|} \frac{\Delta_i^2}{\Delta_i^2 + \operatorname{Var}[\hat{Q}_{\pi,n}^{hi}(s^{hi}, a_1)] + \operatorname{Var}[\hat{Q}_{\pi,n}^{hi}(s^{hi}, a_i)]}$ .

284 2.  $Pr(a_1 = \operatorname{argmax}_{a \in \mathcal{A}} \hat{Q}_{\pi,n}^{MFMC}(s^{hi}, a)) \geq \prod_{i=2}^{|\mathcal{A}|} \frac{\Delta_i^2}{\Delta_i^2 + (1-\rho_{s,a_1}^2)\operatorname{Var}[\hat{Q}_{\pi,n}^{hi}(s^{hi}, a_i)] + (1-\rho_{s,a_i}^2)\operatorname{Var}[\hat{Q}_{\pi,n}^{hi}(s^{hi}, a_i)]}$ .

285 Notice that when  $|\rho_{s,a_2}| \rightarrow 1$ , the lower bound in the result of Theorem 2 approaches 1, which  
 286 means that the correct greedy action  $a_1$  can be selected with certainty when the reduced-variance  
 287 multifidelity estimator (7) is adopted. Combining the results of Theorems 1 and 2, the proposed  
 288 MFMCRL algorithm is expected to outperform its single high-fidelity Monte Carlo counterpart in terms  
 289 of learning a better policy under a given budget of high-fidelity environment interactions.

## 290 4 Numerical experiments

291 In this section we empirically evaluate the performance of the proposed MFMCRL algorithm on  
 292 synthetic MDP problems and on a NAS use case. Our codes and all experimental details can be found  
 293 in Appendix C.

294 **4.1 Synthetic MDPs**

295 We synthesize multifidelity random MDP problems with state space cardinality  $|\mathcal{S}|$  and action space  
 296 cardinality  $|\mathcal{A}|$ . The high-fidelity transition and reward functions,  $\mathcal{P}^{\text{hi}}$  and  $\mathcal{R}^{\text{hi}}$ , respectively, are  
 297 first generated based on a random process as detailed in Appendix C.2. Next, for a given  $\mathcal{P}^{\text{hi}}$  and  
 298  $\mathcal{R}^{\text{hi}}$ , the corresponding  $\mathcal{P}^{\text{low}}$  and  $\mathcal{R}^{\text{low}}$  are generated by injecting Gaussian noise to meet a desired  
 299 signal-to-noise ratio. Specifically, we generate a random matrix  $\mathcal{P}_N$  of size  $|\mathcal{S}| \times |\mathcal{A}| \times |\mathcal{S}|$  from  
 300 a normally distributed r.v. with mean 0 and variance  $\sigma_{\mathcal{P}}^2$ , and set  $\mathcal{P}^{\text{low}} = \mathcal{P}^{\text{hi}} + \mathcal{P}_N$ .  $\mathcal{P}^{\text{low}}$  is then  
 301 appropriately normalized so that  $\sum_{s^{lo'} \in \mathcal{S}} \mathcal{P}^{\text{lo}}(s^{lo'} | s^{\text{lo}}, a) = 1$ . Similarly, we generate a random  
 302 matrix  $\mathcal{R}_N$  of size  $|\mathcal{S}| \times |\mathcal{A}|$  from a normally distributed r.v. with mean 0 and variance  $\sigma_{\mathcal{R}}^2$  and set  
 303  $\mathcal{R}^{\text{low}} = \mathcal{R}^{\text{hi}} + \mathcal{R}_N$ .  $\mathcal{P}^{\text{hi}}$  and  $\mathcal{R}^{\text{hi}}$  are then encapsulated within a gym-like environment with which  
 304 the agent can interact by exchanging sample tuples of the form  $(s^{\text{hi}}, a, r^{\text{hi}}, s^{\text{hi}'})$ . Similarly,  $\mathcal{P}^{\text{lo}}$  and  
 305  $\mathcal{R}^{\text{lo}}$  are encapsulated within a gym-like environment to form the low-fidelity environment. In this  
 306 experiment, both low- and high-fidelity environments share the same state-action space—that is,  $\mathcal{T}$  is  
 307 an identity transformation—yet the transition and reward functions of the low-fidelity environment  
 308 are different since they are corrupted with noise. Notice that even if the agent could draw an infinite  
 309 number of samples from  $\mathcal{P}^{\text{lo}}$  and  $\mathcal{R}^{\text{lo}}$ , it would not be able to recover  $\mathcal{P}^{\text{hi}}$  and  $\mathcal{R}^{\text{hi}}$  since  $\mathcal{P}^{\text{lo}}$  and  
 310  $\mathcal{R}^{\text{lo}}$  underneath the low-fidelity environment themselves are corrupted. This situation mimics what  
 311 happens in practice when we attempt to learn  $\mathcal{P}^{\text{lo}}$  and  $\mathcal{R}^{\text{lo}}$  based on real data and build an RL  
 312 environment off those learned functions to train the agent.

313 After constructing the multifidelity environments, we train an RL agent using the proposed MFCRL  
 314 algorithm over 10K high-fidelity episodes, where a training episode is defined to be a trajectory that  
 315 ends at a terminal state. The MFCRL agent interacts with the low-fidelity environment as shown in  
 316 Algorithm 1, to generate reduced-variance estimates of the state-action value function. As a baseline  
 317 for comparison, we train another RL agent (MCRL) using the standard the first-visit MC control  
 318 algorithm over 10K high-fidelity episodes [34]. We set  $\gamma$  and  $\epsilon$  to 0.99 and 0.1, respectively. Every 50  
 319 training episodes, the greedy policy w.r.t to the estimated  $Q$  function is used to test the performance  
 320 of the agent on 200 test episodes. We repeat the whole experiment with 36 different random seeds  
 321 (to fully leverage our 36 core machine) and report the mean and standard deviation (across different  
 322 seeds) of the test episode rewards in Figure 2(a). One can observe that for a given budget of high-  
 323 fidelity episodes, the proposed MFCRL algorithm outperforms MCRL in terms of policy performance,  
 324 with performance improving as the RL agent collects more low-fidelity samples ( $\# \tau^{\text{lo}}$  refers to the  
 325 number of low-fidelity trajectories started from a state-action pair). In Figure 2(b), we vary the SNR  
 326 of the low-fidelity environment and observe that performance improves as SNR increases. This  
 327 is expected because the low- and high-fidelity environments are better-correlated at higher SNRs.  
 328 Notice that when the SNR of the low-fidelity environment is -10 dB, there is no benefit from doing  
 329 multifidelity RL. The reason is that the low- and high-fidelity environments are too weakly correlated  
 330 to benefit from multifidelity estimation. In fact, for this case  $\mathbb{E}_{s,a,s'}[|\mathcal{P}^{\text{hi}} - \mathcal{P}^{\text{lo}}|] = 0.275 \pm 0.33$ , and  
 331  $\mathbb{E}_{s,a}[|\mathcal{R}^{\text{hi}} - \mathcal{R}^{\text{lo}}|] = 1.029 \pm 0.024$ , compared with the other extreme case (SNR +3dB) for which  
 332  $\mathbb{E}_{s,a,s'}[|\mathcal{P}^{\text{hi}} - \mathcal{P}^{\text{lo}}|] = 0.009 \pm 0.0002$ , and  $\mathbb{E}_{s,a}[|\mathcal{R}^{\text{hi}} - \mathcal{R}^{\text{lo}}|] = 0.230 \pm 0.006$ . This is also evident  
 333 in Figure 2(c), where we show the mean variance reduction factor  $\text{Var}[\hat{Q}^{\text{MFMC}}]/\text{Var}[\hat{Q}^{\text{hi}}]$  estimated  
 334 based off the last 1K training episodes. When the low-fidelity environment is less noisy (higher SNR),  
 335 more variance reduction can be attained.

336 **4.2 NAS**

337 In NAS, the task is to discover high-performing neural architectures with respect to a given training  
 338 dataset over a predefined search space. While many earlier works attempted to design RL-based NAS  
 339 algorithms, [3, 40, 13], it has since become clear that the sample complexity of RL is too high to be  
 340 competitive with state-of-the-art NAS methods [4, 37]. In this experiment we study how multifidelity  
 341 RL can improve learning in NAS over standard RL, which could serve to catalyze future work in this  
 342 direction to make RL more competitive in NAS.

343 For this experiment we use the tabular dataset of NAS-Bench-201 [10] to construct multifidelity RL  
 344 environments as detailed in Appendix C.3. In summary, the RL agent sequentially configures the  
 345 nodes of an architecture (inducing an MDP), after which the architecture is trained on the training  
 346 dataset for  $L$  epochs, and the validation accuracy on a held-out validation data set is provided to the  
 347 agent as a reward. By maximizing the total rewards, high-performing architectures can be discovered.  
 348 NAS-Bench-201 reports the validation accuracy curves for all the architectures in the search space



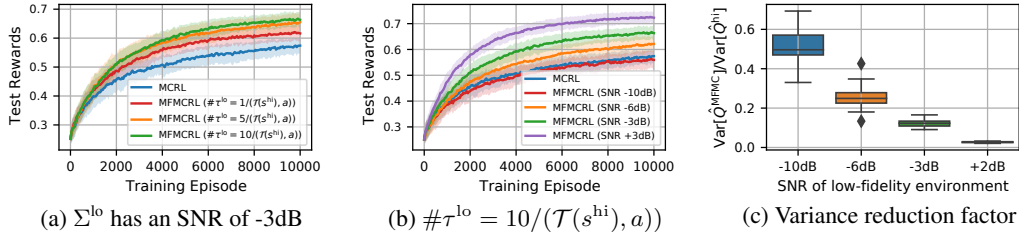


Figure 2: Mean and standard deviation of test episode rewards for the proposed MFCRL during training: (a) test episode rewards improve with increasing number of low-fidelity samples ( $\# \tau^{lo}$ ); (b) test episode rewards improve with less noisy low-fidelity environments; (c) variance reduction factor improves when low- and high-fidelity environments are more correlated. These results are based on a random MDP with  $|\mathcal{S}| = 200$ ,  $|\mathcal{A}| = 8$ .

349 as a function of the number of training epochs  
 350 and for three image data sets. We construct two  
 351 multifidelity scenarios as follows. In both scenarios,  
 352 the validation accuracy of an architecture at the end  
 353 of training (i.e. at  $L = 200$  epochs) is used as a  
 354 high-fidelity reward in the high-fidelity environment.  
 355 For the low-fidelity environment, we have two cases:  
 356 (i) low-fidelity environment is identical to the  
 357 high-fidelity environment except for the reward function,  
 358 which is now the validation accuracy at the  $L = 10$   
 359 th training epoch, and (ii) low-fidelity environment  
 360 is defined for a smaller search space and the reward  
 361 function is the validation accuracy of an architecture  
 362 at the  $L = 10$ th training epoch. Note that in case  
 363 (ii) the state space and dynamics differ between the  
 364 low- and high-fidelity environments. For both cases,  
 365 we train both our proposed MFCRL and the MCRL  
 366 exactly as we did in Section 4.1, and we report the  
 367 mean and standard deviation of test episode rewards  
 368 in Figure 3. We can observe that our multifidelity  
 369 RL framework does indeed improve over standard RL  
 and that performance gains are higher when the low- and high-fidelity environments are more similar, case (i).

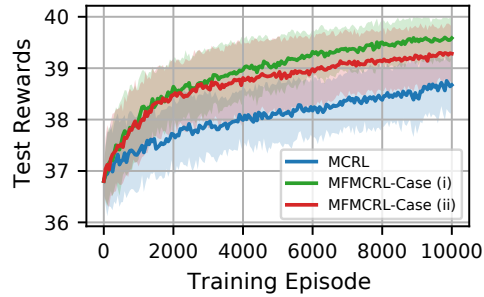


Figure 3: Mean and standard deviation of test episode rewards for the proposed MFCRL during training on multifidelity NAS environments. See text for description of the two multifidelity scenarios (i) and (ii). In both cases,  $\# \tau^{lo} = 5/(\mathcal{T}(s^{hi}), a)$ .

## 370 5 Conclusion

371 In this paper we have studied the RL problem in the presence of a low- and a high-fidelity environment  
 372 for a given control task, with the aim of improving the agent’s performance in the high-fidelity  
 373 environment with multifidelity data. We have proposed a multifidelity estimator based on the method  
 374 of control variates, which uses low-fidelity data to reduce the variance in the estimation of the  
 375 state-action value function. The impacts of variance reduction on policy improvement and policy  
 376 evaluation are theoretically analyzed, and a multifidelity Monte Carlo RL algorithm (MFCRL) is  
 377 devised. We show that for a finite budget of high-fidelity data, the MFCRL agent can well exploit the  
 378 cross-correlations between low- and high-fidelity data and yield superior performance. In our future  
 379 work, we will study the design of a control-variate-based multifidelity RL framework with function  
 380 approximation to solve continuous state-action space RL problems.

## 381 6 Broader impact

382 *Positive impacts:* The energy/cost associated with generating low-fidelity data is generally much  
 383 smaller than that of high-fidelity data. By leveraging low-fidelity data to improve the learning of RL  
 384 agents, greener agents are realized. *Negative impacts:* Running multifidelity RL agent training with  
 385 weakly-correlated low- and high-fidelity environments can be wasteful of resources since the benefits  
 386 in this case are not significant.

387 **References**

- 388 [1] Pieter Abbeel, Morgan Quigley, and Andrew Y Ng. Using inaccurate models in reinforcement  
389 learning. In *Proceedings of the 23rd international conference on Machine Learning*, pages 1–8,  
390 2006.
- 391 [2] Eitan Altman. *Constrained Markov decision processes*, volume 7. CRC Press, 1999.
- 392 [3] Bowen Baker, Otkrist Gupta, Nikhil Naik, and Ramesh Raskar. Designing neural network  
393 architectures using reinforcement learning. *arXiv preprint arXiv:1611.02167*, 2016.
- 394 [4] Prasanna Balaprakash, Romain Egele, Misha Salim, Stefan Wild, Venkatram Vishwanath,  
395 Fangfang Xia, Tom Brettin, and Rick Stevens. Scalable reinforcement-learning-based neural  
396 architecture search for cancer deep learning research. In *Proceedings of the International  
397 Conference for High Performance Computing, Networking, Storage and Analysis*, pages 1–33,  
398 2019.
- 399 [5] Richard Bellman. A Markovian decision process. *Journal of Mathematics and Mechanics*,  
400 6(5):679–684, 1957.
- 401 [6] S.N. Bernstein. On a modification of Chebyshev’s inequality and of the error formula of Laplace.  
402 *Ann. Sci. Inst. Sav. Ukraine, Sect. Math. 1*, 4(5), 1924.
- 403 [7] Dimitri P Bertsekas et al. *Dynamic programming and optimal control: Vol. 1*. Athena Scientific  
404 Belmont, 2000.
- 405 [8] Yevgen Chebotar, Ankur Handa, Viktor Makoviychuk, Miles Macklin, Jan Issac, Nathan Ratliff,  
406 and Dieter Fox. Closing the sim-to-real loop: Adapting simulation randomization with real  
407 world experience. In *2019 International Conference on Robotics and Automation (ICRA)*, pages  
408 8973–8979. IEEE, 2019.
- 409 [9] Mark Cutler, Thomas J Walsh, and Jonathan P How. Real-world reinforcement learning via  
410 multifidelity simulators. *IEEE Transactions on Robotics*, 31(3):655–671, 2015.
- 411 [10] Xuanyi Dong and Yi Yang. NAS-Bench-201: Extending the scope of reproducible neural  
412 architecture search. *arXiv preprint arXiv:2001.00326*, 2020.
- 413 [11] M Giselle Fernández-Godino, Chanyoung Park, Nam-Ho Kim, and Raphael T Haftka. Review  
414 of multi-fidelity models. *arXiv preprint arXiv:1609.07196*, 2016.
- 415 [12] Tuomas Haarnoja, Aurick Zhou, Pieter Abbeel, and Sergey Levine. Soft actor-critic: Off-  
416 policy maximum entropy deep reinforcement learning with a stochastic actor. In Jennifer Dy  
417 and Andreas Krause, editors, *Proceedings of the 35th International Conference on Machine  
418 Learning*, volume 80 of *Proceedings of Machine Learning Research*, pages 1861–1870. PMLR,  
419 10–15 Jul 2018.
- 420 [13] Yesmina Jaafra, Jean Luc Laurent, Aline Deruyver, and Mohamed Saber Naceur. A review  
421 of meta-reinforcement learning for deep neural networks architecture search. *arXiv preprint  
422 arXiv:1812.07995*, 2018.
- 423 [14] Michael Janner, Justin Fu, Marvin Zhang, and Sergey Levine. When to trust your model: Model-  
424 based policy optimization. *Advances in Neural Information Processing Systems*, 32:12519–  
425 12530, 2019.
- 426 [15] Sham Kakade and John Langford. Approximately optimal approximate reinforcement learning.  
427 In *In Proc. 19th International Conference on Machine Learning*. Citeseer, 2002.
- 428 [16] Lodewijk Kallenberg. Markov decision processes. *Lecture Notes. University of Leiden*, 2011.
- 429 [17] Michael Kearns, Yishay Mansour, and Andrew Y Ng. A sparse sampling algorithm for near-  
430 optimal planning in large Markov decision processes. *Machine Learning*, 49(2):193–208,  
431 2002.

- 432 [18] Sami Khairy, Ruslan Shaydulin, Lukasz Cincio, Yuri Alexeev, and Prasanna Balaprakash.  
433 Learning to optimize variational quantum circuits to solve combinatorial problems. In *AAAI*,  
434 pages 2367–2375, 2020.
- 435 [19] Phaedon-Stelios Koutsourelakis. Accurate uncertainty quantification using inaccurate computa-  
436 tional models. *SIAM Journal on Scientific Computing*, 31(5):3274–3300, 2009.
- 437 [20] Christiane Lemieux. Control variates. *Wiley StatsRef: Statistics Reference Online*, pages 1–8,  
438 2014.
- 439 [21] Shibo Li, Wei Xing, Robert Kirby, and Shandian Zhe. Multi-fidelity Bayesian optimization via  
440 deep neural networks. *Advances in Neural Information Processing Systems*, 33, 2020.
- 441 [22] Timothy P Lillicrap, Jonathan J Hunt, Alexander Pritzel, Nicolas Heess, Tom Erez, Yuval Tassa,  
442 David Silver, and Daan Wierstra. Continuous control with deep reinforcement learning. *arXiv*  
443 *preprint arXiv:1509.02971*, 2015.
- 444 [23] Timothy A Mann and Yoonsuck Choe. Directed exploration in reinforcement learning with  
445 transferred knowledge. In *European Workshop on Reinforcement Learning*, pages 59–76.  
446 PMLR, 2013.
- 447 [24] Xuhui Meng and George Em Karniadakis. A composite neural network that learns from multi-  
448 fidelity data: Application to function approximation and inverse PDE problems. *Journal of*  
449 *Computational Physics*, 401:109020, 2020.
- 450 [25] Volodymyr Mnih, Koray Kavukcuoglu, David Silver, Andrei A Rusu, Joel Veness, Marc G  
451 Bellemare, Alex Graves, Martin Riedmiller, Andreas K Fidjeland, Georg Ostrovski, et al.  
452 Human-level control through deep reinforcement learning. *Nature*, 518(7540):529–533, 2015.
- 453 [26] Benjamin P Moster, Thorsten Naab, Magnus Lindström, and Joseph A O’Leary. GalaxyNet:  
454 connecting galaxies and dark matter haloes with deep neural networks and reinforcement  
455 learning in large volumes. *Monthly Notices of the Royal Astronomical Society*, 507(2):2115–  
456 2136, 2021.
- 457 [27] Benjamin Peherstorfer, Karen Willcox, and Max Gunzburger. Optimal model management for  
458 multifidelity Monte Carlo estimation. *SIAM Journal on Scientific Computing*, 38(5):A3163–  
459 A3194, 2016.
- 460 [28] Benjamin Peherstorfer, Karen Willcox, and Max Gunzburger. Survey of multifidelity methods  
461 in uncertainty propagation, inference, and optimization. *Siam Review*, 60(3):550–591, 2018.
- 462 [29] Paris Perdikaris, Maziar Raissi, Andreas Damianou, Neil D Lawrence, and George Em  
463 Karniadakis. Nonlinear information fusion algorithms for data-efficient multi-fidelity mod-  
464 elling. *Proceedings of the Royal Society A: Mathematical, Physical and Engineering Sciences*,  
465 473(2198):20160751, 2017.
- 466 [30] Julian Schrittwieser, Ioannis Antonoglou, Thomas Hubert, Karen Simonyan, Laurent Sifre, Si-  
467 mon Schmitt, Arthur Guez, Edward Lockhart, Demis Hassabis, Thore Graepel, et al. Mastering  
468 Atari, Go, chess and shogi by planning with a learned model. *Nature*, 588(7839):604–609,  
469 2020.
- 470 [31] John Schulman, Sergey Levine, Pieter Abbeel, Michael Jordan, and Philipp Moritz. Trust region  
471 policy optimization. In *International conference on Machine Learning*, pages 1889–1897.  
472 PMLR, 2015.
- 473 [32] John Schulman, Filip Wolski, Prafulla Dhariwal, Alec Radford, and Oleg Klimov. Proximal  
474 policy optimization algorithms. *arXiv preprint arXiv:1707.06347*, 2017.
- 475 [33] Varun Suryan, Nahush Gondhalekar, and Pratap Tokekar. Multifidelity reinforcement learning  
476 with Gaussian processes: model-based and model-free algorithms. *IEEE Robotics & Automation*  
477 *Magazine*, 27(2):117–128, 2020.
- 478 [34] Richard S Sutton and Andrew G Barto. *Reinforcement learning: An introduction*. MIT Press,  
479 2018.

- 480 [35] Matthew E Taylor and Peter Stone. Transfer learning for reinforcement learning domains: A  
481 survey. *Journal of Machine Learning Research*, 10(7), 2009.
- 482 [36] Matthew E Taylor, Peter Stone, and Yaxin Liu. Transfer learning via inter-task mappings for  
483 temporal difference learning. *Journal of Machine Learning Research*, 8(9), 2007.
- 484 [37] Colin White, Willie Neiswanger, and Yash Savani. Bananas: Bayesian optimization with neural  
485 architectures for neural architecture search. *arXiv preprint arXiv:1910.11858*, 1(2):4, 2019.
- 486 [38] Christopher K Williams and Carl Edward Rasmussen. *Gaussian processes for machine learning*,  
487 volume 2. MIT Press, Cambridge, MA, 2006.
- 488 [39] Zhuangdi Zhu, Kaixiang Lin, and Jiayu Zhou. Transfer learning in deep reinforcement learning:  
489 A survey. *arXiv preprint arXiv:2009.07888*, 2020.
- 490 [40] Barret Zoph and Quoc V Le. Neural architecture search with reinforcement learning. *arXiv*  
491 *preprint arXiv:1611.01578*, 2016.

## 492 Checklist

- 493 1. For all authors...
- 494 (a) Do the main claims made in the abstract and introduction accurately reflect the paper’s  
495 contributions and scope? [Yes] See Figure 1.
- 496 (b) Did you describe the limitations of your work? [Yes] Refer to Section 4.1
- 497 (c) Did you discuss any potential negative societal impacts of your work? [Yes] Refer to  
498 Section 6.
- 499 (d) Have you read the ethics review guidelines and ensured that your paper conforms to  
500 them? [Yes]
- 501 2. If you are including theoretical results...
- 502 (a) Did you state the full set of assumptions of all theoretical results? [Yes] Refer to the  
503 theorem statements in Section 3.3.
- 504 (b) Did you include complete proofs of all theoretical results? [Yes] Refer to Appendix B.
- 505 3. If you ran experiments...
- 506 (a) Did you include the code, data, and instructions needed to reproduce the main experi-  
507 mental results (either in the supplemental material or as a URL)? [Yes] Our codes are  
508 included in the supplemental materials and will be shared online after a decision is  
509 made on the manuscript.
- 510 (b) Did you specify all the training details (e.g., data splits, hyperparameters, how they  
511 were chosen)? [Yes] Refer to Section 4 and Appendix C.
- 512 (c) Did you report error bars (e.g., with respect to the random seed after running experi-  
513 ments multiple times)? [Yes] See Figures 2 and 3.
- 514 (d) Did you include the total amount of compute and the type of resources used (e.g., type  
515 of GPUs, internal cluster, or cloud provider)? [Yes] Refer to Appendix C.1.
- 516 4. If you are using existing assets (e.g., code, data, models) or curating/releasing new assets...
- 517 (a) If your work uses existing assets, did you cite the creators? [Yes] Refer to Section 4.2.
- 518 (b) Did you mention the license of the assets? [No] The dataset used in this work is  
519 publicly available under the MIT License.
- 520 (c) Did you include any new assets either in the supplemental material or as a URL? [No]  
521 Synthetic data used in Section 4.1 can be regenerated by using the codes we provided.
- 522 (d) Did you discuss whether and how consent was obtained from people whose data you’re  
523 using/curating? [N/A]
- 524 (e) Did you discuss whether the data you are using/curating contains personally identifiable  
525 information or offensive content? [N/A]
- 526 5. If you used crowdsourcing or conducted research with human subjects...

527  
528  
529  
530  
531  
532

- (a) Did you include the full text of instructions given to participants and screenshots, if applicable? [N/A]
- (b) Did you describe any potential participant risks, with links to Institutional Review Board (IRB) approvals, if applicable? [N/A]
- (c) Did you include the estimated hourly wage paid to participants and the total amount spent on participant compensation? [N/A]